INTERNATIONAL JOURNAL OF LATEST TECHNOLOGY IN ENGINEERING, MANAGEMENT & APPLIED SCIENCE (IJLTEMAS)

ISSN 2278-2540 | DOI: 10.51583/IJLTEMAS | Volume XIII, Issue X, October 2024

Characterization of Palm Kernel Shell Ash Nanoparticles as Coating Material for High Temperature Applications.

EA Abhulimen, TN Guma, N Achara

Mechanical Engineering Department, Nigerian Defence Academy, Kaduna, Nigeria

DOI : https://doi.org/10.51583/IJLTEMAS.2024.131012

Received: 22 October 2024; Accepted: 30 October 2024; Published: 07 November 2024

Abstract: The kernel shell of oil palm (Elaesis guineensis) was milled, calcinated and synthesized into nanoparticles (np) with a view to analyzing and ascertaining its high temperature strength. The synthesized particles were characterized to reveal their elemental composition and temperature of maximal decomposition/destruction, with the solgel method employed in the nanoparticle synthesis. The morphology of the Palm Kernel Shell Ash nanoparticles (PKSAnp) viewed from Transmission Electron Microscope (TEM) revealed that the nanoparticles were solid in nature but vary in sizes with some spherical particles visible, and an average particle size found to be 39.17nm. The Electron Dispersion Spectroscope (EDS) result shows that only elements such as C, O, Si, Al, Ca, and K are present in the PKSAnp, with silicon (Si) found to be dominant. Oxides of Silicon and Aluminum (SiO_2 and Al_2O_3) were identified as the key chemical compounds in PKSAnp from X-Ray Fluorescence (XRF) investigation whereas K_2O, CaO and Na_2O were among the other oxides present in traces. The Thermogravimetric analysis (TGA) curve shows a lower proportion of breakdown and a residual weight stability at temperatures above 1000°C, coinciding with the silica content in PKSAnp. This is comparable and consistent with known high temperature coating materials in previous literature.

Key words: Characterization, Palm Kernel Shell, Nanoparticles, Coating, High Temperature

I. Introduction

The Palm Kernel Shell (PKS) is produced by a species of palm, commonly called the Africa oil palm (Elaeis guineensis). It is the hard part that enclosed the nut of palm kernel fruit and the shell parts obtained as residual waste after crushing and removal of nut in the palm oil mill during the extraction of kernel. The use of *Elaeis guineensis* leaves extract as corrosion inhibitor [1], is an established indication that its shell could yield positive result in the management of hot corrosion. The palm kernel shell has estimated value of about 34.5% of a single ripe, fresh fruit [2][3], where in the year 2001 alone, the estimated value of 3.06 million metric tons was produced by Indonesia and Malaysia. From this estimated value of 34.5% PKS from a single fruit, it could be established that the disposal of these biomass wastes will continue to pose major environmental problems [4]. Coating on the other hand refers to a covering applied to the surface of an object, usually the substrate for either a decorative purpose, functional purpose or both [5]. Coatings such as Paints and lacquers mostly serve dual purposes of protection and decoration on the substrate. Some artists' paints are only for decoration whereas the paint on large industrial pipes is for corrosion prevention and identification. Functional coatings may be applied to change the surface properties of a substrate, such as adhesion, wettability, corrosion resistance, or wear resistance [6]. Thermal barrier coatings (TBC) are high-temperature coating systems for metallic surfaces which serve to protect the parts by limiting the thermal exposure of structural components and thus extending their lifetime. A thin coating or thick layer produced either by metallurgical, mechanical, physical, or chemical means alters the surface of a manufactured item to achieve certain desired property [7]. The process often results in improved appearance, adhesion, corrosion resistance, tarnishes resistance, chemical resistance and wear resistance. The use of protective thermal barrier and bond coatings has resulted in significant improvements in superalloy performance.

II. Materials, Equipment and Methods

A. Materials

The materials used in the course of this work include; Palm kernel shell sourced from Ohordua in Edo State, Nigeria, De-ionized water, Distilled water, Hydrochloric Acid (HCl), Sodium Hydroxide (NaOH), ethanol, Zinc Sulphate $ZnSO_4$, and a Cationic Surfactant (N, N-dimethyldodecylamine).

B. Equipment

The Equipment used include; Erlenmeyer flask, copper grid, Metal mould, hydraulic press, Rockwell hardness, grinding and polishing machine, TEM (Jeol, JSM2010), graphite crucible, Carbolite electric resistance furnace ASAP 2020 Micromeritics surface area analyzer, PANalytical X-PERT PRO diffractometer, Nanoparticle size analyzer Model: HORIBA LB 550, Perkin Elmer spectrum 100 FT – IR spectrometer, pulverizing machine, X-ray diffraction machine (XRD), Fourier transform infrared spectrometry (FTIR), Q50 thermogravimetric analyzer, Perkin Elmer differential scanning calorimeter (DSC7), magnetic stirrer, rectifier

C. Methods

The methods employed in the research are as enumerated below:

ISSN 2278-2540 | DOI: 10.51583/IJLTEMAS | Volume XIII, Issue X, October 2024

1) *Palm Kernel Shell Ash Processing*: The palm kernel shell so sourced (Figure 1: The PKS) was cleaned and dried and the dry PKS were in a high-intensity ball milling machine, crushed and milled as in Figure 2: PKS undergoing crushing, into powdered particles which were placed in a graphite crucible and heated to 1200°C in a Carbolite electric resistance furnace to create Palm Kernel Shell Ash (PKSA).

Figure 1: The PKS

Figure 2: PKS undergoing crushing

2) *PKSA Nanoparticles Production:* The Palm Kernel Shell Ash nanoparticles (PKSAnp) utilized in this study were made using the sol gel technique. 50 grams of NaOH was dissolved in 1dm^3 of water to treat the PKSA particles. This sodium hydroxide solution was added to the PKSA. The fluid was covered with Erlenmeyer flask and agitate for two hours. The solution was then filtered and the carbon residue removed. The filtrate was cooled to room temperature. With the addition of HCl, it was stirred continually until the pH reached 7, after which it was aged for 8hrs at 65^{0}C to produce gel. When the gel layers had formed in the solution, the stirring was halted. The collected layers were centrifuged at 6000g for 5mins to separate the pellets which were washed with distilled water and ethanol solution. The filtered pellets were then dried in a professional oven for 30mins at 80^{0}C and then ground into powder using a mortar and pestle.

D. Characterization of the PKSA Nanoparticles

1) *Transmission Electron Microscopy (TEM):* TEM (Jeol, JSM2010) (see Figure 3.3) was used to analyze the particle size and shape of the generated nanoparticles. 10mg sample of nanoparticles was sonicated in 5ml of isopropyl alcohol for 3hrs. Using a dropper, the sample solution was applied to the copper grid that had been coated with carbon (The sample chamber was emptied before the copper grid was added to the apparatus) and left to cure at room temperature. The number averaged particle radius was used to calculate the particle size on the presumption that the particle was spherical and the sample was photographed after being scanned along a 200kV electron beam on the sample placed on a carbon-coated copper grid in a vacuum operated in the 10^{-9} Torr range at 25^0 maximum tilt angle in goniometer with single and double tilt stages [8].

2) *X-Ray Diffractometer (XRD) Analysis:* The X-ray diffraction (XRD) patterns of the PKSAnp samples were acquired using a Cu K radiation-powered XRD diffractometer, LR39487C (40kV, 40mA). made by XPertPro PANalytical. The small angle stepwise rise was 0.01^0 across the 1 to 8^0 range, and the broad angle stepwise increase was 1^0, 2 min^{-1} over the 8 to 90^0 range, respectively. Using the Scherrer's equation[9],

$$D\frac{K\lambda}{\beta Cos\theta} = \qquad (2.1)$$

ISSN 2278-2540 | DOI: 10.51583/IJLTEMAS | Volume XIII, Issue X, October 2024

Where θ is the angle between the incident and diffracted beams (degree), *β;* is the line broadening at half the maximum intensity, after subtracting the instrumental line broadening (rad.), D; the particle size of the sample (nm), λ the is wavelength of the X-ray and K is a dimensionless shape factor, with a value close to unity; the samples' particle size was estimated.

3) *Thermal Analysis:* Using a TA Instrument TGA Q50 thermogravimetric analyzer, the thermal decomposition was measured in terms of global mass loss. The mass loss was measured as a function of temperature with a precision of 0.1. The samples were placed loosely in an open sample pan of 6.4mm diameter and 3.2mm depth with an initial sample weight of 8-10mg. Using a heating rate of 10^0C/min, the temperature was controlled to rise from room temperature (25^0C) to 1000^0C. At room temperature and atmospheric pressure, high quality Argon was constantly pumped into the furnace at a flow rate of 60ml/min to purge the furnace for 30mins before the commencement of each run to create an inert atmosphere and ward off any unintended oxidative breakdown. With the TA Instruments' universal analysis 2000 software, the TG and DTA curves were derived. In addition, a Perkin Elmer differential scanning calorimeter (DSC7) was used to accurately measure the melting points, glass transitions, and heats of fusion. The typical temperature range was from 10 to 400^0C and the temperature scale was calibrated using a two-point calibration, measuring the onset temperatures of indium and zinc standards. The enthalpy scale was also calibrated using the observed delta-H from an accurately known amount of indium[10].

4) *Composition analysis:* The generated nanoparticles' elements were analyzed using a Mini Pal small Energy Dispersive X-Ray Fluorescence Spectrometer (EDXRF) with a computer running the specialized Mini Pal analysis software serving as the system's controller. EDXRF spectrometer is the elemental analysis tool of choice, for many applications, in that it is smaller, simpler in design and relatively cost effective in operation. It has a very high-count rates and comparatively high energy resolution. Samples were provided as thin films on a reflective carrier and the primary beam struck the sample at a glancing angle of less than 0.1^0 under total-reflection conditions. Silicon drift detectors measured the energy of an incoming photon by the amount of ionization it produced in the detector material and a transversal field was generated by a series of ring electrodes that forces charge carriers to 'drift' to a small collection electrode. The calibration was performed by a set of elemental and multi elemental standards whereas the analysis and quantification were performed by the addition of a suitable Internal Standard (IS) to the sample. The elemental concentration was determined based on the analytical signals of the analyte and their respective instrumental sensitivities [11].

III. Results And Discussion

The physical, morphology, chemical composition, and thermal characteristics of the PKSA nanoparticles are as discussed and the findings of the characterization experiments provided below;

A. TEM Image of the Palm kernel Shell Nanoparticles (PKSAnp)

Figure 3: morphology of the PKSAnp and Fig. 4 depict the morphology of the PKSAnp as seen by TEM. It was discovered that the nanoparticles were solid in nature but varied in size. Particles with a spherical form were also visible. The average particle sizes obtained are 39.07np. It was noted that C, O, Si, Al, Ca, and K were found in the EDS as the PKSAnp underwent micro-analysis. The higher peak of silicon (Si) in figure 3.2 was caused by silica, which makes up the majority of PKSAnp.

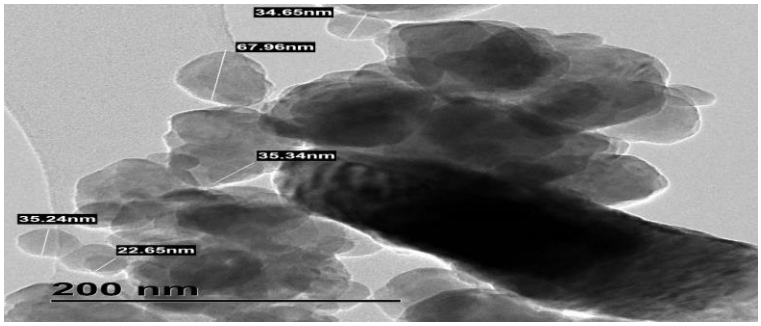

Figure 3: morphology of the PKSAnp

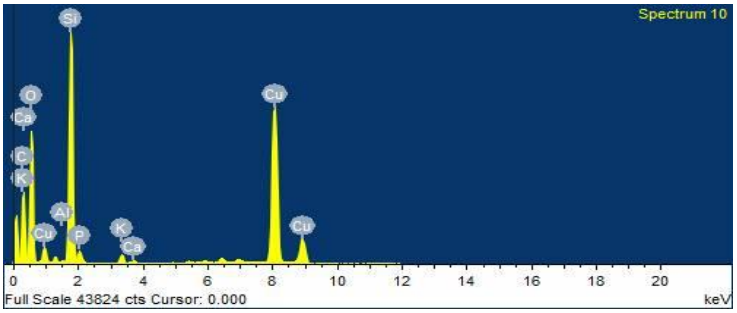

Figure 4: TEM/EDS of the PKSAnp

ISSN 2278-2540 | DOI: 10.51583/IJLTEMAS | Volume XIII, Issue X, October 2024

B. X-ray Fluorescence (XRF) Analysis of the PKSA Nanoparticles

Table 1 displays the PKSAnp's XRF chemical composition. SiO_2 and Al_2O_3 were identified as key components of the PKSAnp by XRF investigation with K_2O, CaO and Na_2O being among the other oxides that were shown to be present in traces.

Table 1: Composition of the PKSA nanoparticles

Compounds	SiO_2	Al_2O_3	Fe_2O_3	CaO	MgO	Na_2O	K_2O	LOI
PKSAnp	83.17	8.67	0.9	2.32	1.3	0.21	0.2	2.01

C. XRD Analysis of the Palm Kernel Shell Nanoparticles (PKSAnp)

The PKSAnp's XRD pattern showed that its major diffraction peaks are at 31.44°, 24.6°, 59.9°, 71.2° and 83.7°; corresponding to those from standard silicon[12] with their inter-planar distances being 3.31A, 4.20A°, 1.89A°, 1.57A°, and 1.37A°. This is in good agreement with the Joint committee on powder diffraction standard (JCPDS) data belonging to high temperature materials [13] and the phases present at these peaks being quartz (SiO_2), and Aluminum Phosphate ($AlPO_4$) as shown in fig. 5 and tables 2 and 3 respectively. According to the XRD study, silica has the greatest proportion of all the compounds present. The wide X-ray diffraction pattern shown that PKSAnp is amorphous materials. This is consistent with findings in other biomass ash samples[14]. The pick broadening pattern indicates no tacking faults, microstrain, and other defects in the crystal structure whereas the observed broad hump and the Full Width at Half Maximum, FWHM suggests that the synthesized materials are nanocrystalline in nature with very small particle size.

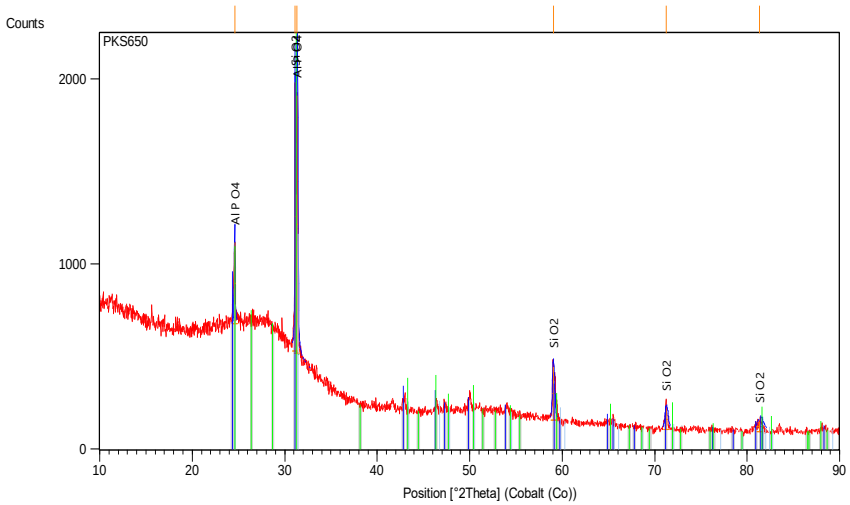

Figure 5: XRD pattern of PKSAnp

D. TGA/DTA of the Palm kernel Shell Nanoparticles (PKSAnp)

"Derivatograph OD 102," DTA measurements were logged at a 10°C/min argon heating rate. Figure 6 6 shows the findings of the DTA/TGA scan of the PKSA nanoparticles. The Thermogravimetric analysis (TGA) curve shows a lower proportion of breakdown and a residual weight stability at temperatures above 1000°C, coinciding with the silica content in PKSAnp. After the sample was heated to near 1000°C, the sample began to breakdown with the decomposed byproducts comprising silica. The PKSAnp was found to be more thermally stable as a result of the silica, which delayed the degrading process. The significant differences in Tm and ΔH indicate stability and structural conformation. This is comparable and consistent with known high temperature coating materials in previous literature.

Table 2: Peak List

Pos. [°2Th.]	Height [cts]	FWHM Left [°2Th.]	d-spacing [Å]	Rel. Int. [%]	Tip Width	Matched by
24.586840	439.166600	0.102336	4.20421	30.19	0.1228	01-076-0229
31.142640	1454.510000	0.076752	3.33468	100.00	0.0921	01-085-0794
31.349440	1396.110000	0.127920	3.31323	95.98	0.1535	01-076-0229
59.028710	286.298400	0.204672	1.81705	19.68	0.2456	01-085-0794
71.226970	108.047700	0.307008	1.53723	7.43	0.3684	01-085-0794
81.344260	55.742470	0.818688	1.37350	3.83	0.9824	01-085-0794

ISSN 2278-2540 | DOI: 10.51583/IJLTEMAS | Volume XIII, Issue X, October 2024

Table 3: Identified Patterns List

Visible	Ref. Code	Score	Compound Name	Displacement [°2Th.]	Scale Factor	Chemical Formula
*	01-085-0794	45	Silicon Oxide	0.000	0.737	SiO_2
*	01-076-0229	33	Aluminum Phosphate	0.000	0.804	$AlPO_4$

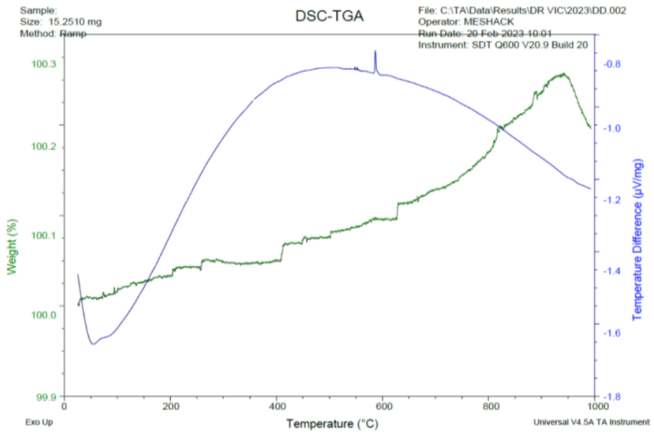

Figure 6: TGA/DTA of the PKSAnp

IV. Conclusion

Palm kernel shell ash nanoparticles were effectively characterized as coating material for high temperature application. The Electron Dispersion Spectroscope (EDS) result shows that only elements such as C, O, Si, Al, Ca, and K are present in the PKSAnp, with silicon (Si) found to be dominant. Oxides of Silicon and Aluminum (SiO_2 and Al_2O_3) were identified as the key chemical compounds in PKSAnp from X-Ray Fluorescence (XRF) investigation whereas K_2O, CaO and Na_2O were among the other oxides present in traces**.** The Thermogravimetric analysis (TGA) curve shows a lower proportion of breakdown and a residual weight stability at temperatures above 1000°C. This is comparable and consistent with known high temperature coating materials in previous literature.

References

1. Abhulimen. EA, (2018). "An investigation on the optimal concentration of oil palm (elaeis guineensis) leaves extract as corrosion inhibitor of carbon steel in deaerated saline solution," MOJ Applied Bionics and Biomechanics, vol. 2, no. 2, pp. 109–113. doi: 10.15406/mojabb.2018.02.00050.
2. Skawinska A. and Jagustyn, B., (2013). Evaluation of physicochemical properties of palm kernel shell as agro biomass used in the energy industry.," CHEMIK, vol. 67, pp. 552–559.
3. Oladosu, K.O., Kareem B., Akinnuli B.O. and Alade A.O. (2016). "Optimization of ash yield from the combustion of palm kernel shell and selected additives (Al2O3, CaO and MgO) using D-optimal design. Leonardo Electron.," J. Pract. Technol, vol. 15, pp. 9–18.
4. Ikumapayi O. M. and Akinlabi E. T., (2018) Composition, Characteristics and Socioeconomic benefits of palm kernel shell exploitation-an overview. Asian Network for Scientific Information, vol.11, no.5 pp.220–232. doi: 10.3923/JEST.2018.220.232.
5. Howarth G. A. and Manock H. L., (1997). Water-borne polyurethane dispersions and their use in functional coatings," Surface Coatings International, vol. 80, no. 7, pp. 324–328 doi: 10.1007/bf02692680.
6. Coating – Retrieved from https://en.wikipedia.org/wiki/Coating, Accessed Sep. 13, 2021.
7. JEOL (2010) TEM Overview of the Metal FUJJI Industry. Access; September 10 2024. Available: https://www.google.com/search?q=JEOL+(2010)+TEM
8. Electron Nanoscopy Instrumentation Facility." https://ncmn.unl.edu/enif/about/jeol_2010.shtml. Accessed Apr. 20, 2023.
9. Patterson A. L., (1939). "The Scherrer Formula for X-Ray Particle Size Determination," Phys. Rev., vol. 56, no. 10, pp. 978–982. doi: 10.1103/PhysRev.56.978.
10. Experimental Method and Testing Procedures - Laboratory 10: Thermogravimetric Analysis. Accessed Apr. 20, 2023). https://sites.google.com/a/iastate.edu/laboratory-10-thermogravimetric-analysis/experimental-methods.
11. Marguí E., Queralt I., and E. de Almeida, (2022). X-ray fluorescence spectrometry for environmental analysis: Basic principles, instrumentation, applications and recent trends," Chemosphere, vol. 303, p. 135006, Sep., doi: 10.1016/J.CHEMOSPHERE.2022.135006.

ISSN 2278-2540 | DOI: 10.51583/IJLTEMAS | Volume XIII, Issue X, October 2024

12. Patra S., Mitra P., and Pradhan S. K., (2011). Preparation of nanodimensional CdS by chemical dipping technique and their characterization," Materials Research, vol. 14, no. 1, pp. 17–20, doi: 10.1590/S1516-14392011005000015.
13. "JCPDS--International Centre for Diffraction Data - LC Linked Data Service: Authorities and Vocabularies | Library of Congress." https://id.loc.gov/authorities/names/n78034812.html. Accessed May 16, 2023.
14. Prusty J. K., Patro S. K., and Basarkar S. S., (2016). Concrete using agro-waste as fine aggregate for sustainable built environment – A review," International Journal of Sustainable Built Environment, vol. 5, no. 2, pp. 312–333. doi: 10.1016/J.IJSBE.2016.06.003.